Supporting Information

Role of Acid Mixtures Etching on the Surface Chemistry and Sodium Ion Storage in $Ti_3C_2T_x$ MXene

Mark Anayee[ax], Narendra Kurra[ax], Mohamed Alhabeb[a], Mykola Seredych[a], Mohamed Nejib Hedhili[c], Abdul-Hamid Emwas[c], Husam N. Alshareef[b], Babak Anasori[a] and Yury Gogotsi[a†]

[a]A. J. Drexel Nanomaterials Institute, and Department of Materials Science and Engineering, Drexel University, Philadelphia, PA 19104, USA

[b]Materials Science and Engineering, Physical Science & Engineering Division, King Abdullah University of Science and Technology (KAUST), Thuwal, 23955-6900, Saudi Arabia

[c]Core Labs, King Abdullah University of Science and Technology (KAUST), Thuwal, 23955-6900, Saudi Arabia

[x] These authors contributed equally to this work

† Corresponding author. E-mail: gogotsi@drexel.edu

Experimental Section

All chemicals were used as received, without further purification. Layered ternary carbide Ti_3AlC_2 (MAX phase) powder was produced by Carbon-Ukraine, *Ltd*, with particle size < 40 µm.

Synthesis of $Ti_3C_2T_x$ MXene. Multilayered $Ti_3C_2T_x$ MXene powders were synthesized by etching Ti_3AlC_2 MAX phase with 5 wt% hydrofluoric acid aqueous solutions. Three different etchants, HF, HF/HCl and HF/H_2SO_4 were used for etching the MAX phase in order to remove Al atoms. Three separate diluted acids in polypropylene bottles were prepared as follows: (i) 9 mL of H_2O (DI water), (ii) 6 mL of concentrated HCl (37 wt%, Fisher Scientific) was added to 3 mL of H_2O, and (iii) 1.5 mL concentrated H_2SO_4 (95wt.%, Fisher Scientific) was added to 7.5 mL H_2O. To each separate bottle (i-iii), 1 mL of concentrated HF (48-51 wt%, Across Organics) was added under constant stirring. 1 g of Ti_3AlC_2 powder was slowly added into each bottle under stirring (400 rpm) and the reaction temperature was set at 40 °C. The etching reaction was continued for 15 h and washing was conducted with deionized (DI) water via repeated centrifugation for 5 minutes at 3500 rpm (2450 rcf). Colorless acidic supernatant was decanted after each wash and washing continued until neutral pH, > 6, was reached. Then, multilayer MXene samples were collected using vacuum filtration over a polyvinylidene fluoride (PVDF) membrane with a pore size of 0.45 µm (Milipore Durapore, HVLP04700). We attempted to eliminate the influence of surface adsorbed water layers (physisorbed) on the *d*-spacing of MXenes by drying all samples under vacuum at 200 °C for 12 h and minimizing residence time in ambient conditions. However, due to the intrinsic hydrophilic nature of MXenes, adsorption of moisture from the atmosphere was still possible. Therefore, $Ti_3C_2T_x$ samples obtained by HF, HF/HCl and HF/H_2SO_4 are referred to as $Ti_3C_2T_x$ (HF), $Ti_3C_2T_x$ (HF/HCl), $Ti_3C_2T_x$ (HF/H_2SO_4), respectively.

Regarding the etchant constitution, the pH / concentration of H^+ were calculated to be 1.37 / 0.04 M for (HF), -0.86 / 7.30 M for (HF/HCl), and -0.45 / 2.80 M for (HF/H_2SO_4). The primary

factor used to normalize the three etchants is that the HF concentration is the same in all cases, 5 wt%. Concentration of H^+ could influence the structure and surface termination of MXenes slightly, as discussed in the main and supporting texts, likely due to the saturated concentration of H^+ ions in each etchant.

Material Characterization

X-ray photoelectron spectroscopy (XPS). The chemical composition of the MXene powder samples was analyzed using high resolution XPS. XPS studies were carried out in a Kratos Axis Ultra DLD spectrometer (Kratos Analytical, Manchester, UK) equipped with a monochromatic Al Kα X-ray source ($h\nu$ = 1486.6 eV) operating at 150 W, a multichannel plate and delay line detector under a vacuum of 10^{-8} mbar. The survey and high-resolution spectra were collected at fixed analyzer pass energies of 160 eV and 20 eV, respectively and quantified using empirically derived relative sensitivity factors provided by Kratos analytical. Samples were mounted in a floating mode in order to avoid differential charging. Charge neutralization was required for all samples. Binding energies were referenced to the C 1*s* peak of (C-C, C-H) bond which was set at 284.8 eV. The data were analyzed with commercially available software, CasaXPS, using linear background shapes and mixed Gaussian Lorentzian peak shapes.

Nuclear Magnetic Resonance (NMR) spectroscopy. ^{13}C NMR spectra were acquired using a Bruker 400 MHz AVANACIII NMR spectrometer equipped with 4 mm Bruker MAS probe (BrukerBioSpin, Rheinstetten, Germany). The samples were finely ground with KBr (Fisher Scientific) then packed evenly into a 4 mm zirconia rotor and sealed at the open end with a Vespel cap. The spectra were recorded with 14 kHz spinning rate using one pulse program with 30° flipping angle. To achieve high signal to noise ratio, the spectra were recorded by collecting at least 24,000 scans with recycle delay time of 10 s. Bruker Topspin 3.2 software (Bruker BioSpin, Rheinstetten, Germany) was used to collect and analyze the data. ^{19}F and ^{1}H NMR spectra were recorded using Bruker 600 MHz AVANACIII NMR spectrometer equipped with triple resonance 2.5 mm Bruker MAS probe (BrukerBioSpin, Rheinstetten, Germany). ^{19}F NMR spectra were recorded with 4,000 scans while ^{1}H NMR spectra were recorded with 1,000 scans at room temperature. The spinning rate for all experiments was set to 30 kHz using one pulse program (z_g) from Bruker pulse library.

Characterization Techniques. Structural characteristics of MAX and MXene were investigated by X-ray diffraction (XRD) using Rigaku Smart Lab (Tokyo, Japan) diffractometer using Cu Kα radiation (voltage and current settings were 40 kV and 44 mA, respectively) with a step scan of 0.04º, 2θ range 3-65º and dwell time of 0.5 s. The morphology of the $Ti_3C_2T_x$ MXene samples was imaged using a scanning electron microscope (SEM) (Zeiss Supra 50VP, Germany). The electrical conductivities of the samples were measured using a four-point probe (ResTest v1, Jandel Engineering Ltd., Bedfordshire, UK) with a probe distance of 1 mm. Thermal analysis-mass spectrometry (TA-MS) measurements were carried out using TA Instruments' thermal analyzer (SDT Q 650, Discovery Series) equipped with a Mass Spectrometer (110/220V) from room temperature to 1500°C at a heating rate of 10 °C/min under a constant helium flow of 100 mL/min. The gas products that evolved during heating were determined by MS and mass/charge (*m/z)* evolution profiles were recorded as a function of temperature. Parts per billion (ppb) sensitivity over the mass range 1-300 *amu* (atomic mass unit; gas dependent) was achieved with a quadrupole detection system, including a closed ion source, triple mass filter, and dual (Faraday and Secondary Electron Multiplier) detector system.

Electrochemical Testing. Coin cells of CR2032 type were assembled in an Ar-filled glove box (Vacuum Technologies Inc., Gloucester, MA) with moisture and O_2 levels below 0.1 ppm. Binder and conductive additive-free $Ti_3C_2T_x$ electrodes were prepared by cold pressing of the multilayered $Ti_3C_2T_x$ powder samples. 100 mg of dried $Ti_3C_2T_x$ powder was cold-pressed using a Carver hydraulic press model 3925 (Carver Inc., Wabash, IN) at a pressure of 1 GPa to form $Ti_3C_2T_x$ pellets. Typical mass loadings were 75 mg/cm^2 with diameter of 13 mm. These pellets were used directly as working electrodes without any additional current collector to investigate the intrinsic electrochemical storage of Na-ions. Na foil was used as counter and reference electrodes after scraping off the surface oxides layer inside the glove box. The electrolyte solution was 1M $NaClO_4$ dissolved in a mixture of ethylene carbonate (EC) and propylene carbonate (PC) with a volume ratio of 1:1, in which 5 vol% fluoroethylene carbonate (FEC) was added as an electrolyte additive. It was reported that the electrolyte additive FEC has a film forming property, in particular for Na-ion batteries, capable to stabilize the electrochemical performance by reducing the decomposition of PC.[1] Glass microfiber (Whatman) membrane saturated with the electrolyte (~0.1 mL) was employed as an electronic insulating separator between the working electrode and Na metal foil. The coin cells were sealed by a crimping machine (MTI Corporation) in an Ar-filled glove box after all the components were stacked and aligned. Cells were conditioned for 4 h in a static state at room temperature prior to electrochemical testing, to induce sufficient wetting of electrodes and separator. Cyclic voltammetry (CV) was conducted using VMP3 (Biologic, France) between 0.01 and 3.0 V versus Na^+/Na at different scan rates. Gravimetric, areal, and volumetric capacities/capacitances were calculated based on the weight, area, and volume of active material, respectively.

Calculations. Gravimetric specific capacitance, C_m (F/g), of electrode materials was calculated from the CV curves by integrating the discharge portion using the following equation:

$$C_m = \frac{1}{\mathrm{V}mv}\int idV \quad (1)$$

where i is the current (mA), V is the potential window (V), v is the scan rate (mV/s), and m is the mass of the active material (mg).

Areal capacitance was estimated by multiplying the gravimetric capacitance (C_m) with areal mass loading (mg/cm^2). Capacity values were estimated by the following formula:

$$\text{Specific capacity} = \int it \quad (2)$$

where the integration is done over the discharge portion of the *i*-*t* curve.

Capacity values were normalized by weight, area, and volume of the electrodes.

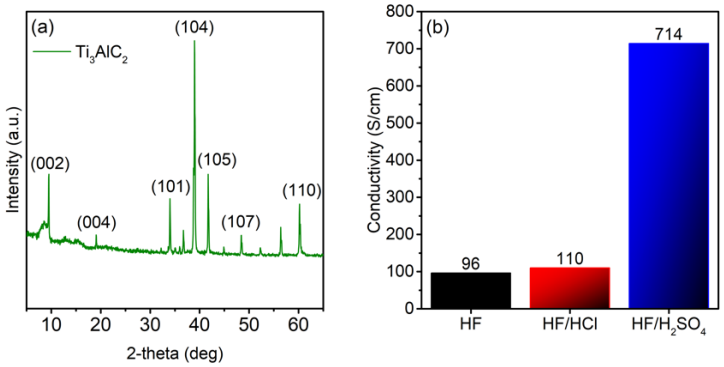

Fig. S1 XRD pattern of Ti_3AlC_2 MAX phase (a) and four-point probe electrical conductivity values of $Ti_3C_2T_x$ multilayer pellets (b).

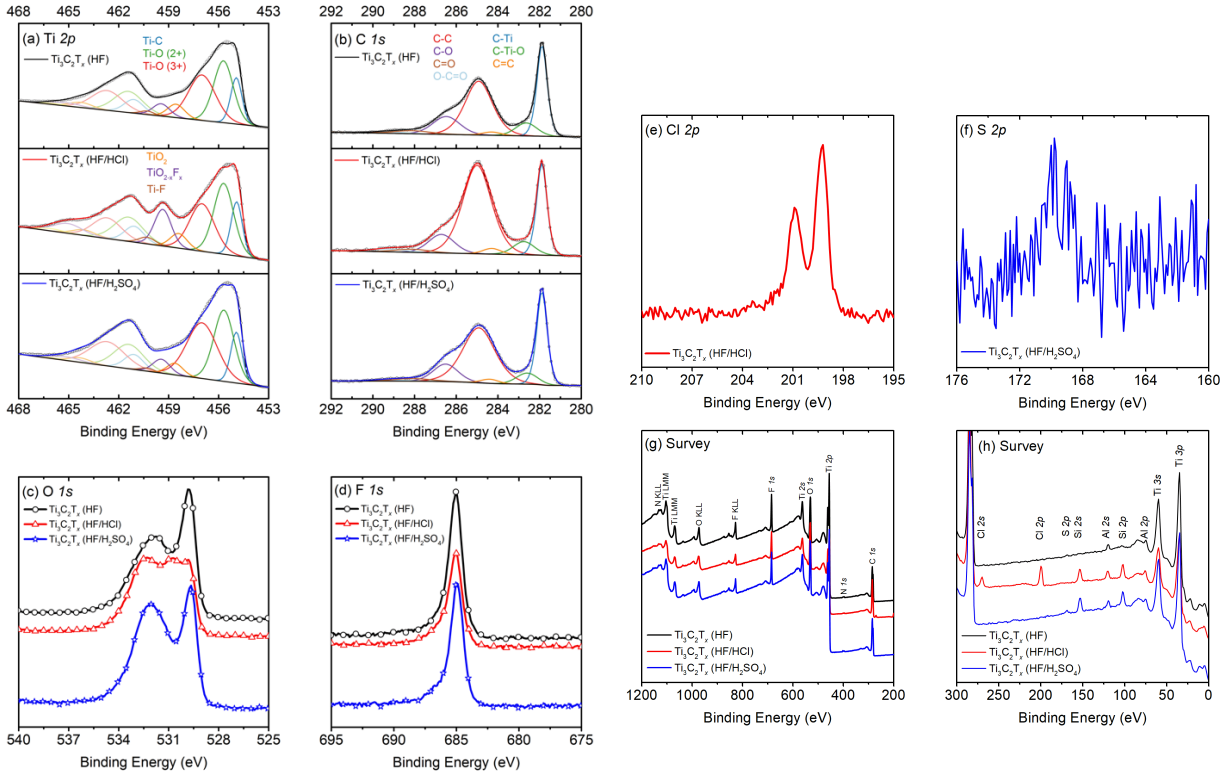

Fig. S2 Core-level X-ray photoelectron spectra of Ti 2*p* (a), C 1*s* (b), O 1*s* (c) and F 1*s* (d) of $Ti_3C_2T_x$ (HF), $Ti_3C_2T_x$ (HF/HCl), $Ti_3C_2T_x$ (HF/H_2SO_4) powder samples, represented with black (top), red (middle) and blue (bottom) colored graphs, respectively. Cl 2*p* for $Ti_3C_2T_x$ (HF/HCl) (e) and S 2*p* for $Ti_3C_2T_x$ (HF/H_2SO_4) (f). Survey-level spectra for all samples split into two binding energy ranges for clarity; high (g) and low (h), respectively.

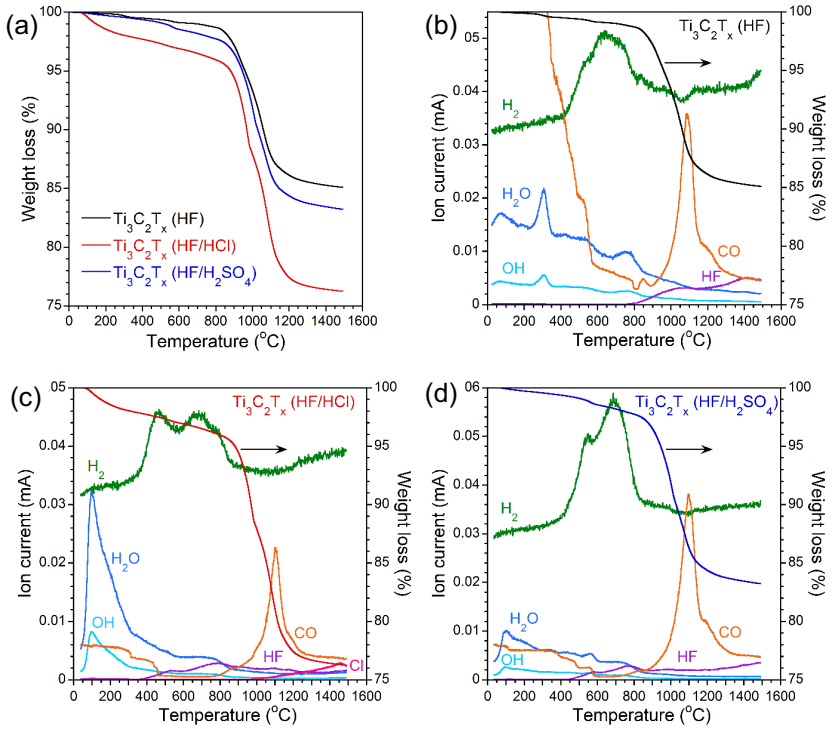

Fig. S3 TA-MS analysis for $Ti_3C_2T_x$ obtained by etching Ti_3AlC_2 in different acids environment: (a) Comparison of TG curves; (b-d) *m/z* thermal profiles for $Ti_3C_2T_x$ etched in HF (b), HF/HCl (c) and HF/H_2SO_4 (d).

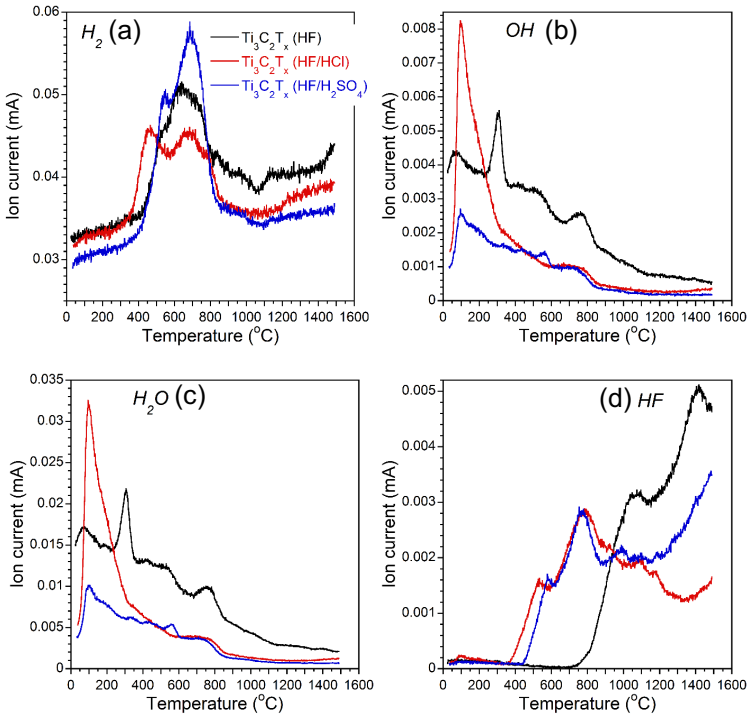

Fig. S4 Mass spectrometry data for $Ti_3C_2T_x$ obtained by etching Ti_3AlC_2 in different acid environments: H_2 (a), OH (b), H_2O (c) and HF (d).

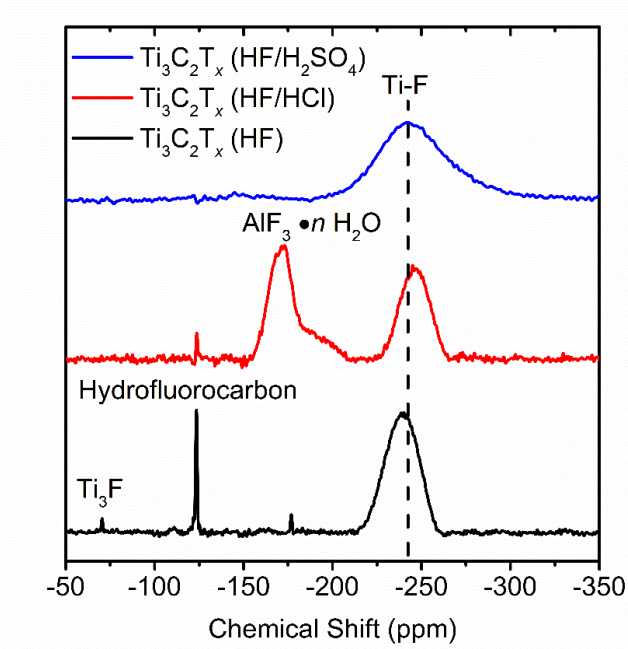

Fig. S5 ^{19}F NMR spectra for $Ti_3C_2T_x$ (HF) (black, bottom), $Ti_3C_2T_x$ (HF/HCl) (red, middle), and $Ti_3C_2T_x$ (HF/H_2SO_4) (blue, top).

Discussion

X-ray photoelectron spectroscopy. In order to investigate the surface functionality and chemical composition of the $Ti_3C_2T_x$ samples, X-ray photoelectron spectroscopy (XPS) measurements were carried out on all three samples. Survey spectra shown in Figs. S2g-h confirmed the presence of Ti, C, O, F and Al elements for the $Ti_3C_2T_x$ (HF), $Ti_3C_2T_x$ (HF/HCl) and $Ti_3C_2T_x$ (HF/H_2SO_4) samples. The $Ti_3C_2T_x$ (HF/HCl) sample also contained Cl and the $Ti_3C_2T_x$ (HF/H_2SO_4) sample also contained S. The detected Si in all of the samples is attributed to contamination from the environment and laboratory tools. The elemental composition was obtained by applying the appropriate relative sensitivity factors (RSFs) to the integrated peak areas of specific core level spectra of different elements shown in Fig. S2 and normalizing based on the Ti content. The overall compositions calculated are as follows: $Ti_3C_{2.0}O_{2.3}F_{1.1}Al_{0.1}$ for $Ti_3C_2T_x$ (HF), $Ti_3C_{1.8}O_{3.2}F_{1.2}Cl_{0.2}Al_{0.2}$ for $Ti_3C_2T_x$ (HF/HCl), and $Ti_3C_{1.9}O_{3.2}F_{1.1}S_{0.2}Al_{0.1}$ for $Ti_3C_2T_x$ (HF/H_2SO_4).

The Ti 2*p* core level was fitted with six doublets (Ti $2p_{3/2}$ – Ti $2p_{1/2}$) by a fixed area ratio equal to 2:1 and doublet separation of 5.7 eV (except for Ti – C where the doublet separation is equal to 6.2 eV) as shown in Fig. S2a. The Ti $2p_{3/2}$ components were located at binding energies of 455.0, 455.8, 457.1, 458.6, 459.4 and 460.3 eV. The Ti $2p_{3/2}$ component centered at 455.0 eV is associated with Ti bonded to C.[2] The Ti $2p_{3/2}$ components centered at 455.8 eV and 457.1 eV are attributed to Ti atoms with valence states +2 and +3, which correspond to bonding with O surface terminations, respectively.[2b, 2c, 3] The Ti $2p_{3/2}$ component centered at 458.6 eV is associated with TiO_2, while the Ti $2p_{3/2}$ component centered at 459.4 eV corresponds to $TiO_{2-x}F_x$ species. The Ti $2p_{3/2}$ component centered at 460.3 eV is attributed to C-Ti-F_x bond.[4] In case of $Ti_3C_2T_x$ (HF/HCl), the $TiO_{2-x}F_x$ component is more prominent as compared to that in $Ti_3C_2T_x$ (HF) and $Ti_3C_2T_x$ (HF/H_2SO_4) samples, which is indicative of a higher degree of oxidation and degradation.

As shown in Fig. S2b, C 1*s* core level was fitted with seven components located at 282.0 eV, 282.8 eV, 284.2, 284.8 eV, 286.3, 288.2 and 289.5 corresponding to C-Ti, C-Ti-O, C=C (sp^2),

C-C/C-H (sp^3), C-O, C=O, and O-C=O, respectively.[5] The relative intensity ratios of C-Ti to C-C components are seen different for $Ti_3C_2T_x$ (HF/HCl) when compared to $Ti_3C_2T_x$ (HF) and $Ti_3C_2T_x$ (HF/H_2SO_4) samples. This may be attributed to larger amount of adventitious carbon due to higher propensity of the material to capture carbon adsorbates. Furthermore, presence of TiO_2 species may decrease bonding between Ti and C, leading to decrease of the C-Ti component and increase of the C-C component.

The F 1*s* core level spectra of $Ti_3C_2T_x$ samples, Fig. S2d, did not show significant differences. Furthermore, the concentration of F in the samples was found to be same based on the Ti to F ratio of ~2.6-2.7. Therefore, the anions present in the etchant do not play a role in the extent of fluorination of the MXene. However, in accordance with previous reports, Cl was detected in the $Ti_3C_2T_x$ (HF/HCl) sample, Fig. S2e, which was attributed to Cl surface terminations.[6] Similarly, S was also detected in the $Ti_3C_2T_x$ (HF/H_2SO_4) sample as shown in Fig. S2f. However, the nature of sulfur containing specie or the interaction between it and MXene is not clear at the moment. Quantification and speciation are made difficult due to the high signal-to-noise ratio (SNR) and uncertainty in the background level. However, we attempted to address both aspects. The S2*p* spectrum appears to exhibit a pair of peaks at ~169 and ~170 eV due to spin-orbit splitting of the 2*p* orbital to 3/2 and 1/2 components, respectively. These positions correspond to metal sulfate species which can be attributed to remaining sulfate anions within the interlayer. If sulfur terminations existed, we would expect the peaks to appear close to the binding energy for metal sulfide species, ~161-162 eV. Moreover, rough quantification reveals that the sulfur content is at impurity level. Therefore, we hypothesize that etching with (HF/H_2SO_4) does not lead to sulfur surface terminations and formation of Ti-S bonds.

The O 1*s* core level spectra of $Ti_3C_2T_x$ samples, Fig. S2c, showed a peak around 529.8 eV which can be attributed to oxygen surface terminations located at bridging sites and to TiO_2.[4] However, the broad peak ~532 eV includes the contribution of different species like C-Ti-$(OH)_x$, C-O, C=O, $TiO_{2-x}F_x$, and H_2O.[4] Therefore, we make no attempt to deconvolute the O 1*s* high resolution spectra due to the co-existence of oxygen stemming from multiple sources including $Ti_3C_2T_x$ MXene, TiO_2, adsorbed water, and adventitious carbon which will lead to a high degree of uncertainty. Instead, the total oxygen content of the sample is used for analysis. The atomic ratio of O to F was found to be 2.1 for $Ti_3C_2T_x$ (HF) while it goes up to 2.8 for $Ti_3C_2T_x$ (HF/HCl) and $Ti_3C_2T_x$ (HF/H_2SO_4) samples. In the case of $Ti_3C_2T_x$ (HF/HCl) sample, the increase can be attributed to partial oxidation of the sample as evidenced by the large TiO_2 peak at ~459 eV in the Ti *2p* spectra. In the case of $Ti_3C_2T_x$ (HF/H_2SO_4) sample, since the ratio of C-C to C-Ti is approximately the same as in the $Ti_3C_2T_x$ (HF) sample, the amount of adventitious carbon present is likely the same and not the cause for the increased amount of oxygen. Furthermore, since no increase in the amount of oxidation was found in the $Ti_3C_2T_x$ (HF/H_2SO_4) sample compared to $Ti_3C_2T_x$ (HF), decomposition of the material is likely not the cause of the increase in O to F ratio. Therefore, the additional oxygen may correspond to a higher concentration of oxygen surface terminations. Overall, since XPS analysis was conducted on freshly prepared samples, aging effects due to oxidation from the environment are minimized.

Thermogravimetric Analysis. Thermogravimetric analysis results presented in Fig. S3a show thermal stability of $Ti_3C_2T_x$ etched in the different acidic environments with the onset temperature for degradation at around 850 ºC, 880 ºC and 900 ºC for $Ti_3C_2T_x$ etched with HF, HF/HCl and HF/H_2SO_4, respectively, suggesting that the stability of MXenes etched with acids mixture is improved. The weight loss between 850 – 1200 ºC associated with the thermal decomposition of MXenes (CO gas evolution) is 12 wt%, 18 wt% and 13 wt% for $Ti_3C_2T_x$ etched

with HF, HF/HCl and HF/H_2SO_4, respectively. A comparison of the MS data for $Ti_3C_2T_x$ obtained by etching in different acid environments is shown in Figs. S3b-d. Significant changes in the intensity of the regions corresponding to hydroxyl groups (–OH), fluoride terminations, and structural water is seen, suggesting their different surface chemistry. As shown in the specific MS in Fig. S4c, the largest amount of H_2O released is for $Ti_3C_2T_x$ etched with HF/HCl, while for $Ti_3C_2T_x$ etched with HF/H_2SO_4 it is the smallest. This can be explained by the larger interlayer distance in the $Ti_3C_2T_x$ sample etched with HF/HCl compared to the samples etched with HF and HF/H_2SO_4, which is in agreement with the XRD results. It is important to note that for all MXenes there is significant contributions from the hydrogen thermal desorption (Fig. S4a).

Nuclear Magnetic Resonance. For the $Ti_3C_2T_x$ multilayered powder samples, etching products (AlF_x, Ti_xF, and hydrofluorocarbons) were found presumably trapped in the interlayer space even though the samples were washed thoroughly until reaching neutral pH, based on the ^{19}F NMR spectra (Fig. S5).[6,7] The $Ti_3C_2T_x$ (HF) sample exhibited two sharp peaks at -70 ppm and -120 ppm attributed to titanium fluorides and hydrofluorocarbons, respectively, while the $Ti_3C_2T_x$ (HF/HCl) sample exhibited the hydrofluorocarbon peak in addition to a strong broad signal at -170 ppm attributed to AlF_3. The $Ti_3C_2T_x$ (HF/H_2SO_4) was free of fluoride related etching products. It is worth mentioning that those etching products could be further removed through delamination or additional washing of the multilayer powders thereby removing their influence on the properties of the material. Furthermore, partially etched multilayer stacks, where titanium to aluminum bonding was still present, could be removed by centrifugation as they are inherently heavier than MXene flakes. However, the present materials and etching byproducts are obtained by employing the same extensive washing procedures, which further indicates that progression of the washing process should be monitored not only by pH but also by analytical techniques such as NMR and TG-MS.

References

1. S. Komaba, T. Ishikawa, N. Yabuuchi, W. Murata, A. Ito and Y. Ohsawa, *ACS Appl. Mater. Interfaces*, 2011, **3**, 4165.
2. (a) Y. Dall'Agnese, M. R. Lukatskaya, K. M. Cook, P. L. Taberna, Y. Gogotsi and P. Simon, *Electrochem. Commun.*, 2014, **48**, 118; (b) I. Persson, L. A. Naslund, J. Halim, M. W. Barsoum, V. Darakchieva, J. Palisaitis, J. Rosen and P. O. A. Persson, *2D Mater.*, 2018, **5**, 10; (c) T. Schultz, N. C. Frey, K. Hantanasirisakul, S. Park, S. J. May, V. B. Shenoy, Y. Gogotsi and N. Koch, *Chem. Mat.*, 2019, **31,** 6590.
3. M. C. Biesinger, B. P. Payne, A. P. Grosvenor, L. W. M. Lau, A. R. Gerson and R. S. Smart, *Appl. Surf. Sci.*, 2011, **257**, 2717.
4. J. Halim, K. M. Cook, M. Naguib, P. Eklund, Y. Gogotsi, J. Rosen and M. W. Barsoum, *Appl. Surf. Sci.*, 2016, **362**, 406.
5. (a) Y. F. Liu, H. F. Du, X. Zhang, Y. X. Yang, M. X. Gao and H. G. Pan, *Chem. Commun.*, 2016, **52**, 705; (b) F. Dong, H. Q. Wang and Z. B. Wu, *J. Phys. Chem. C*, 2009, **113**, 16717; (c) L. B. Zhang, G. Y. Chen, M. N. Hedhili, H. N. Zhang and P. Wang, *Nanoscale*, 2012, **4**, 7038; (d) H. Touhara and F. Okino, *Carbon*, 2000, **38**, 241; (e) F. Y. Zhang, S. G. Advani, A. K. Prasad, M. E. Boggs, S. P. Sullivan and T. P. Beebe, *Electrochim. Acta*, 2009, **54**, 4025.
6. J. Lu, I. Persson, H. Lind, J. Palisaitis, M. Li, Y. Li, K. Chen, J. Zhou, S. Du, Z. Chai, Z. Huang, L. Hultman, P. Eklund, J. Rosen, Q. Huang and P. O. A. Persson, *Nanoscale Adv.*, 2019, **1**, 3680.
7. K. Harris, M. Bugnet, M. Naguib, M. W. Barsoum and G. R. Goward, *J. Phys. Chem. C.*, 2015, 119, **24**, 13713.